Chapter 6
One-Dimensional Heat Source Reconstruction Applied to Phase Transforming Superelastic Ni-Ti Wire

Antoine Jury, Xavier Balandraud, Luděk Heller, Eduardo Alarcon, and Miroslav Karlik

Abstract The study deals with the reconstruction of heat sources originating from deformation processes in metals. A one-dimensional method to be applied on wires or bars is introduced and tested on superelastic NiTi wire subjected to force-controlled loading and unloading. Infrared thermography was used for this purpose. Thermal data were then processed by heat source reconstruction technique using a one-dimensional version of the heat diffusion equation. Attention was paid to the identification of the heat exchanges with the specimen's environment, in particular by convection to the air of ambient temperature. The sensitivity of the method to the degree of spatio-temporal filtering was also tested. Finally, the localization of martensitic transformation in superelastic NiTi was evaluated using the proposed method. It is shown that under force-control regime the phase transformation proceeds in two time-shifted bursts, where each of bursts consists in several displaced and nearly simultaneous transforming zones. This transformation sequence is rationalized by fast latent heat release from the transforming zone upon load control regime, which leads to overheating of surrounding zones thus temporarily suppressing their transformation.

Keywords Shape-memory alloy · NiTi · Infrared thermography · Superelasticity · Heat source reconstruction

Introduction

Among the shape memory alloys (SMAs), near-equiatomic nickel-titanium (NiTi) alloys are the most frequently selected in engineering applications [1]. This is due to their attractive functional properties exhibited by these alloys, such as shape memory effects, superelasticity and high damping capacity. These macroscopic properties originate from a diffusionless

A. Jury (✉)
Nuclear Physics Institute of the CAS, Řež, Czech Republic

Institute of Physics of the CAS, Prague, Czech Republic

Czech Technical University in Prague, Faculty of Nuclear Sciences and Physical Engineering, Department of Materials, Prague, Czech Republic

Université Clermont Auvergne, CNRS, SIGMA Clermont, Institut Pascal, Clermont-Ferrand, France
e-mail: jury@fzu.cz

X. Balandraud
Université Clermont Auvergne, CNRS, SIGMA Clermont, Institut Pascal, Clermont-Ferrand, France
e-mail: xavier.balandraud@sigma-clermont.fr

L. Heller · E. Alarcon
Nuclear Physics Institute of the CAS, Řež, Czech Republic

Institute of Physics of the CAS, Prague, Czech Republic
e-mail: heller@fzu.cz; alarcon@fzu.cz

M. Karlik
Czech Technical University in Prague, Faculty of Nuclear Sciences and Physical Engineering, Department of Materials, Prague, Czech Republic

Charles University, Faculty of Mathematics and Physics, Department of Physics of Materials, Prague, Czech Republic
e-mail: miroslav.karlik@fjfi.cvut.cz

solid-solid phase transformation that can be thermally or mechanically induced. According to the thermomechanical heat treatment, environmental conditions (ambient temperature and heat exchange conditions) and mechanical loading (stress level and loading rate), the tensile response of polycrystalline NiTi-based SMAs may exhibit the propagation of phase transformation fronts [2]. The latter were extensively studied in the literature. They were described first in [3] and then investigated in many studies (see for instance [4–7]). The reader is also referred to [8] for details on the origin of these phase transformation fronts.

The stress-induced phase transformation in NiTi wires subjected to tension is usually tracked in-situ by measuring sudden changes of strain and strain rates, both evaluated either integrally using displacement of the testing machine's cross-head, more accurately using clip-on extensometer, or locally using digital image correlation. Thermal Field Measurements (TFM), based on the use of an infrared (IR) camera [4–6, 9–11] are an alternative way of tracking in-situ the phase transformation in NiTi. In general, TFM takes advantage of temperature changes that always accompany material stretching due to thermomechanical couplings and intrinsic dissipation: thermoelastic coupling, latent heat due to solid-solid phase change, self-heating due to plasticity, viscosity or fatigue damage. The reconstruction of heat sources from temperature changes is possible by using the heat diffusion equation, which in the case of wires can be reduced into 1-D considering axial symmetry and seeking for heat sources integrally over the entire wire cross-section. By *heat source*, we mean the heat power density produced or absorbed by the material itself (i.e. not due to conduction, convection and radiation). To the best knowledge of the authors, one dimensional heat source reconstruction has never been carried out on NiTi subjected to force controlled tensile loadings. In fact, the phase transformation in NiTi normally proceeds under a constant plateau-stress but it cannot under the force controlled loading regime as the latent heat of rapidly transformed zones increases the temperature of their surroundings where the phase transformation may be temporarily suppressed. It may lead to sudden bursts and arrests of the phase transformation along the wire axis appear in NiTi wire. Hence, superelastic NiTi subjected to the force controlled regime represents a perfect example case for present work aiming at the development and testing of a method for one-dimensional reconstruction of heat sources evolving dynamically in time and heterogeneously in space.

The paper is divided into three sections as follows. The first section provides the general background on 1D heat source reconstruction. The second section presents the NiTi material experimental set-up. Finally, results are given and discussed in the third section, with a focus on the spatio-temporal features of phase change fronts along the NiTi wire during a load-unload cycle.

Methodology for Heat Source Reconstruction

Materials produce or absorb heat when subjected to mechanical loadings. As indicated in the introduction, heat sources are defined as the heat power densities (in W m^{-3}) resulting in a temperature changes. In metals, heat is produced or absorbed as a consequence of different deformation and chemical processes. For instance, the thermomechanical coupling upon elastic deformation in metals, called thermoelasticity, results in a heat production inversely proportional to the applied stress rate. On the other hand, phenomena related to energy dissipation such as plasticity, viscosity, fatigue damage always results in irreversible heat production. In NiTi, an additional thermomechanical coupling is involved: a production or absorption of latent heat associated with the austenite-to-martensite or martensite-to-austenite phase changes, respectively. Using the heat diffusion equation, heat sources can be reconstructed from the temperature fields captured by IR thermography at the specimen surface [10–17]. In the present study, we used the so-called 1D approach [10, 13, 14] for reconstructing the heat sources of NiTi wires subjected to force-controlled tensile loadings.

Let us consider a straight NiTi wire whose axial coordinate is denoted z. The simplified local form of the heat equation (6.1) provides the relationship between the temperature change $\Theta(z,t)$ and the heat source $s(z,t)$ (here expressed in °K s^{-1} resulting from its reduction by the product of the density ρ and the specific heat C). The latter quantity is defined with respect to a reference configuration, considered in practice as the unloaded state in thermal equilibrium. The parameter D is the thermal diffusivity of the material (in m^2 s^{-1}) and τ is a characteristic time (in s) characterizing the heat exchanges between the wire lateral surface and its surroundings. The calculation of heat source from the right-hand side of Eq. (6.1) was implemented using derivative Gaussian filters, as detailed in [16].

$$s(z,t) = \frac{d\Theta(z,t)}{dt} + \frac{\Theta(z,t)}{\tau} - D\frac{d^2\Theta(z,t)}{dz^2} \tag{6.1}$$

The characteristic time τ was evaluated from a natural cooling of the sample to ambient temperature after its homogeneous heating without any contact with the jaws of the testing machine. In practice, the specimen was suspended in air with a piece of tape. Figure 6.1a shows the temperature change $\Theta(t)$ during a homogeneous natural return to ambient temperature

after homogeneous heating using a hot air gun. In this way, we consider only the heat exchange of the lateral surface of the specimen with its surroundings. As the heat source is equal to zero (the specimen did not produce heat), Eq. (6.1) becomes:

$$0 = \frac{d\Theta}{dt} + \frac{\Theta}{\tau} \tag{6.2}$$

If τ is a constant, the solution of Eq. (6.2) is a decreasing exponential function of the cooling duration. Assuming that τ may potentially depend on the temperature change Θ, it was proposed to identify the value of $\tau(\Theta)$ for different portions of the curve $\Theta(t)$ as illustrated in Fig. 6.1a. A minimization algorithm was employed with a correlation index equal to 0.995 as stopping criteria. Results are presented in Fig. 6.1b, each point corresponding to the value of τ for a given portion of the curve. A linear equation was identified for the function $\tau(\Theta)$. Figure 6.1c shows the residual heat sources obtained using experimental data. The latter corresponds to the right-hand side of Eq. (6.2) as calculated using the linear fit of $\tau(\Theta)$ (Fig. 6.1b). In fact, the residual heat source values should be equal to zero during this natural return to ambient temperature. The curve in Fig. 6.1c thus provides an estimation of the measurement resolution of the heat source in the case of homogeneous temperature fields: a few tenth of one K s^{-1} at the maximum.
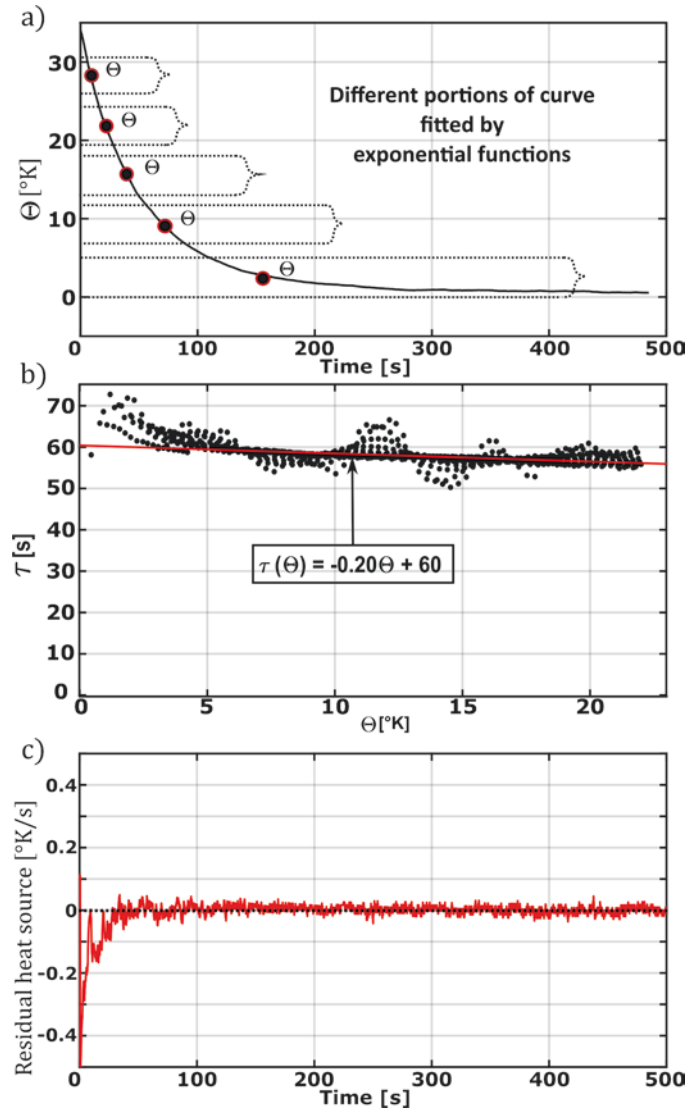
Fig. 6.1 Identification of the characteristic time τ: (**a**) temperature change Θ during a homogeneous natural return to ambient temperature, (**b**) values of τ as a function of Θ, (**c**) residual heat sources obtained after heat source reconstruction

The thermal diffusivity D was measured using a similar approach. We calculated Eq. (6.1) during the natural cooling after a local heating. This time, the specimen was clamped in the jaws of the machine, then heated locally by gently applying a pressure in the middle of the specimen with the fingers. A unique value of D was identified at room temperature equal to 2.7×10^{-6} m^2 s^{-1}, which is in agreement with [15].

Experimental Set-Up

A Cedip Jade III-MWIR infrared camera was employed to capture the temperature fields after calibration in the range [268 K; 333 K]. The mechanical loading was applied with an MTS uniaxial machine equipped with a 15 kN load cell. Figure 6.2a presents a schematic view of the NiTi wire during heat treatment by Joule effect. Figure 6.2b, c show the wire placed in the mechanical test configuration. It can be noticed that two reference elements made of the same material were added on both sides of the mechanically tested specimen: each reference was clamped in a jaw of the testing machine. This experimental device was introduced in [11]. Effects of changes in the specimen's environment during a test can be tracked thanks to these reference elements: change in temperature of the jaws of the testing machine, in temperature and flow of the ambient air, and more generally any change of the testing room conditions (machines, persons, walls, etc.). The NiTi wire and its two reference elements were painted in black to maximize the thermal emissivity, as well as the close environment to limit parasitic reflections: see Fig. 6.2c.

The specimen was a Ni-Ti SMA wire of 1.78 mm of diameter, supplied by Fort Wayne Metals. It was preliminary heat treated by Joule effect using a 50 A current for a period of 3.5 s as presented in [18]. It was then subjected to mechanical training at ambient temperature ($\approx$300 K) for 20 cycles at $\pm$392 N s^{-1} between 20 N and 1984 N. Lengths L1 and L2 in Fig. 6.1a were equal 40 mm and 80 mm, respectively. These lengths were used for both the annealing treatment and the mechanical loadings. The wire is fully austenitic at ambient temperature in the stress-free state.

A tensile test was carried out on the specimen in a force-controlled mode with a rate of $\pm$20 N s^{-1}, and same minimum and maximum forces as for the preliminary mechanical training. The room temperature was 300 K. The spatial resolution of the full-field thermal measurement was equal to 148.5 µm (will be referred to as dz in the following). Recording frequency was set to 162 Hz, leading to a temporal resolution of 6.17 ms (will be referred to as dt). As we are interested in localized phase transformation phenomena (both in time and in space), there is a compromise to be found between measurement resolution (improved by filtering) and spatial/temporal resolution (penalized by filtering and derivation) for the calculation of the heat sources from Eq. (6.1).
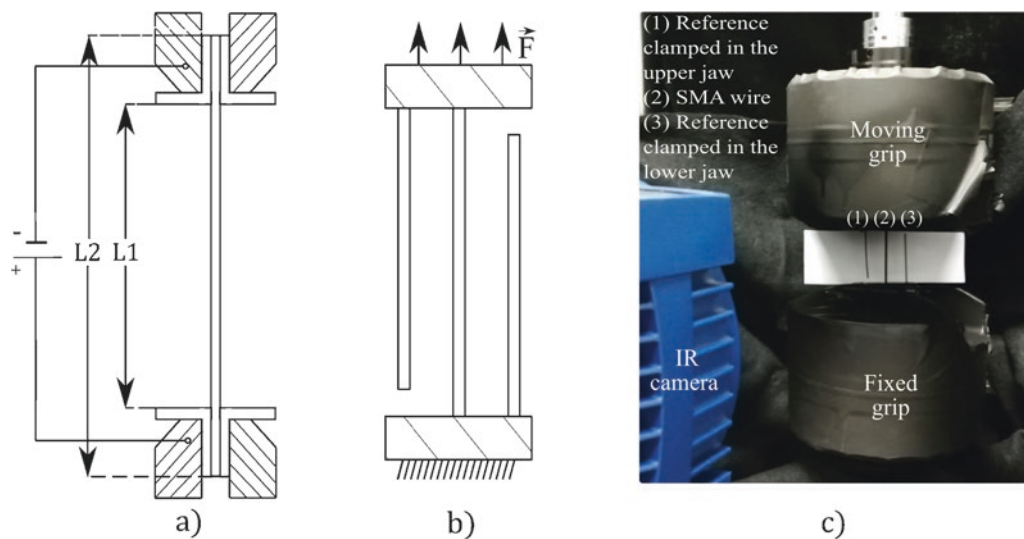
Fig. 6.2 (**a**) Schematic view of the NiTi wire during heat treatment by Joule effect, (**b**) schematic view of the specimen with two reference elements for thermomechanical analysis, (**c**) photo of the specimen and reference elements placed in the jaws of the testing machine

Analysis

Heat source reconstruction was implemented using first-derivative (in time) Gaussian filter in time for the term $d\Theta/dt$ and second-derivative (in space) Gaussian filter in space for the term $d^2\Theta/dz^2$. No filter was applied to the term Θ/τ. Figure 6.3 shows the influence of the standard deviations σ_{space} (in mm) and σ_{time} (in s) of the two Gaussian functions on the spatio-temporal heat source distribution around a short and localized event (see Fig. 6.4 for a global view along the whole duration of the test and the whole length of the wire). The kernel sizes of the convolution windows were set to $\pm 4.5\sigma_{space}$ in space and $\pm 3\sigma_{time}$ in time, i.e. 9 and 6 times the standard deviations respectively. In practice, σ_{space} and σ_{time} were expressed in terms of multiple of the spatial and temporal resolutions of the thermal fields:

$$\sigma_{space} = k_{space}dz \text{ and } \sigma_{time} = k_{time}dt \tag{6.3}$$

where k_{space} and k_{time} are integers.

Figure 6.3a presents the temperature change $\Theta(z,t)$ of a strong calorific event that we used to investigate appropriate filter parameters. Figure 6.3b shows the heat sources that were reconstructed using only a finite difference (FD) scheme
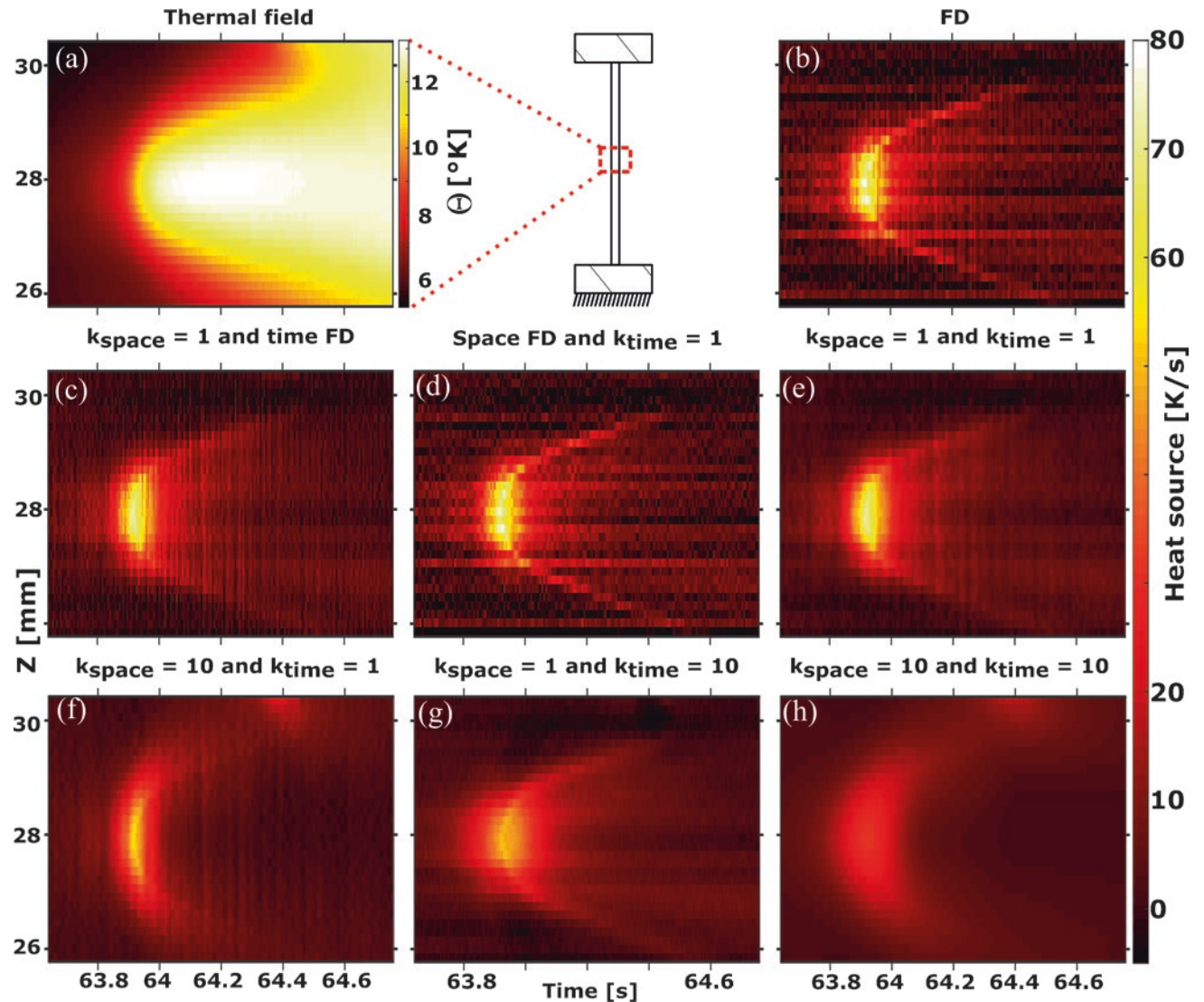
Fig. 6.3 (a) Temperature change Θ around a short and localized calorific event, (c–h) influence of the standard deviations in terms of multiples of spatial (k_{space}) and temporel (k_{time}) resolutions σ_{space} and σ_{time} of the Gaussian derivative filters on the reconstructed heat sources as compared with the solution vie Finite differences (FD) method (b)
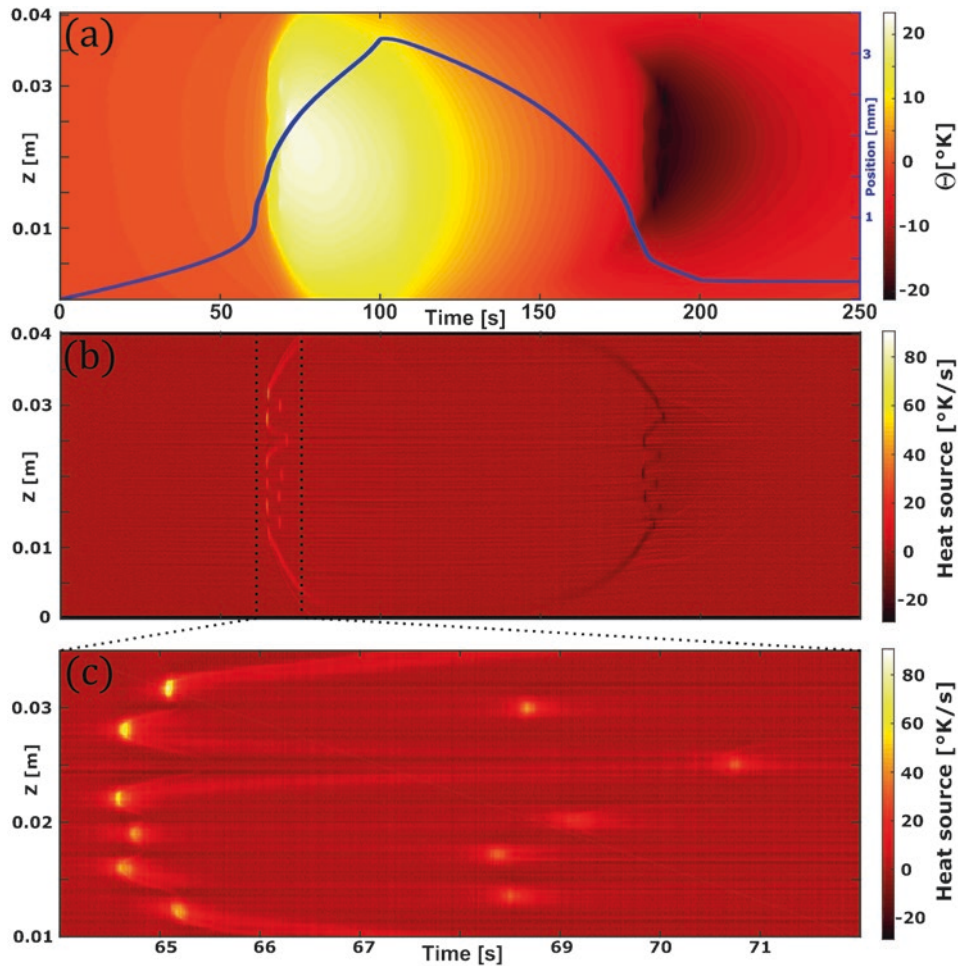
Fig. 6.4 Load-unload cycle: (**a**) temperature change Θ as a function of time and space. The displacement of the actuator is also plotted as a function of time; (**b**) heat source reconstructed from the temperature changes, mapped over the whole duration of the test, (**c**) zoom on the heat source map over the short period revealing strong hear source activity

named forward time centered space of the right-hand side of Eq. (6.1), without filtering. Figure 6.3c–h show the heat sources reconstructed using Gaussian derivation filters for the two derivative terms. It is worth noting that, by construction, heat sources are much more localized in time and in space that the temperatures. Indeed, heat source reconstruction is a physics-based data processing that removes heat exchanges with the specimen surroundings and the heat conduction through the axis of the specimen. It can be also noted that filtering tends to smooth the calorific phenomena. The case for which $\sigma_{space} = dz$ and $\sigma_{time} = dt$ appears to be a good compromise: see Fig. 6.3e. In other words, the advantageous signal-to-noise ratio of the thermal data allows us to apply a "soft" filtering without strongly penalizing the spatial and temporal resolutions of the heat sources. The chosen spatial and temporal resolutions of the reconstructed heat sources are then equal to 1.04 mm and 43.4 ms respectively.

Figure 6.4a presents the temperature change $\Theta(z, t)$, as well as the position of the actuator, as a function of time during the load-unload cycle. Figure 6.4b shows the map of the reconstructed heat source, and Fig. 6.4c shows a zoom over the forward phase transformation (delimited between dotted lines in Fig. 6.4b). The following comments can be made with respect to these graphs.

- Up to approximatively 64 s, the actuator moved quasi-linearly, exhibiting an elastic response of the NiTi wire. Although unseen in Fig. 6.4, the temperature slightly decreased during the first seconds as expected due to thermoelastic coupling: decrease of about 0.02 K in 3.5 s. Then the temperature kept rising continuously and homogeneously up to reach a value of 2 K above the ambient temperature. This increase might be related to premartensitic R-phase transformation, although further investigations are needed to confirm it. It can be noted that the corresponding heat sources of these two phenomena

are not detectable because of the chosen filtering parameters (broader filtering windows would enhance the information about this quasi-homogeneous phenomenon, similar to the so-called zero-dimensional approach [14]).

- From 64 s to 68 s approximatively, the actuator position rate rapidly increased due to the large transformation strain of the stress-induced martensitic transformation. It is accompanied by a strong temperature increase of the wire. This is attributed to the production of latent heat of the phase transformation. Six transformation zones separated by non-transforming zones appeared in less than one second (at around 65 s). Four of the non-transforming zones transformed almost 4 s later, and the last one did it 6 s later. The length of individual transformation zones is ~1.5 mm. Figure 6.3 reveals that the duration of individual transformation zones is shorter than 0.1 s. The burst of an individual transformation zone was followed by two transformation fronts propagating upwards and downwards indicated by inclined heat source traces (covering a total distance of less than 1.5 mm in less than 0.1 s).
- The intensity of the heat sources at the first six transformation zones is two higher than the intensity of the following five.
- It can be noted that continuous propagation of phase transformation fronts also occurred at the two ends of the wire, just after the appearance of the first six martensitic zones (see Fig. 6.4b).
- The reverse transformation, starting at ~150 s, is characterized by heat absorption. The intensity of the heat sources upon the reverse transformation is, however, three times lower than the one observed upon the forward transformation. The differences might be related to other material processed occurring simultaneously upon phase transformations such as plasticity.
- Unlike the forward phase transformation, the reverse transformation initiates inside the clamping jaws. There is not an evident correspondence between the order of activation of the transformation zones upon loading and unloading. The number of localized transformation zones upon the reverse transformation is even lower than upon the forward transformation.

Conclusion

We apply the 1D heat source reconstruction to track the heterogeneous distribution of stress-induced phase transformation in superelastic NiTi upon a force controlled tensile loading-unloading test. Significant temperature changes were observed, as a result of the strong thermomechanical coupling associated supposedly with phase transformations (production and absorption of latent heat). Recorded temperature fields were successfully converted into spatio-temporal evolutions of heat sources associated with forward and reverse martensitic transformation. Attention was paid to the choice of processing parameters with respect to the spatial and temporal resolutions required for a suitable identification of the spatial and temporal kinetics of transformation: rapid nucleation of small martensitic zones and propagation of phase transformation fronts. The method allowed to identify sudden bursts and arrests of phase transformation due to heat effects. In fact, the force controlled loading regime leads to a burst of several phase transformation zones that are displaced due to increasing temperature of their surroundings where the phase transformation is suppressed. These zones can transform only after a sufficient stress increase and/or temperature decrease as a consequence of transformation stress-temperature coupling in NiTi. Consequently, the phase transformation proceeds in two bursts of several displaced transformation zones, where the second burst is shifted in time and related transformation zones fill the non-transformed volume left after the first one.

References

1. C. Otsuka, K. Wayman, *Shape Memory Materials* (Cambridge University Press, Cambridge, 1999)
2. H. Yin, Y. He, Q. Sun, Effect of deformation frequency on temperature and stress oscillations in cyclic phase transition of NiTi shape memory alloy. J. Mech. Phys. Solids **67**, 100–128 (2014)
3. S. Miyazaki, T. Imai, K. Otsuka, Y. Suzuki, Lüders-like deformation observed in the transformation pseudoelasticity of a Ti-Ni alloy. Scr. Metall. **15**, 853–856 (1981)
4. H. Louche, P. Schlosser, D. Favier, L. Orgéas, Heat source processing for localized deformation with non-constant thermal conductivity. Application to superelastic tensile tests of NiTi shape memory alloys. Exp. Mech. **52**(9), 1313–1328 (2012)
5. J.A. Shaw, S. Kyriakides, Thermomechanical aspects of NiTi. J. Mech. Phys. Solids **43**(8), 1243–1281 (1995)

6. J.A. Shaw, S. Kyriakides, Initiation and propagation of localized deformation in elasto-plastic strips under uniaxial tension. Int. J. Plast. **13**(10), 837–871 (1997)
7. J.A. Shaw, S. Kyriakides, On the nucleation and propagation of phase transformation fronts in a NiTi alloy. Acta Mater. **45**(2), 683–700 (1997)
8. P. Sittner, Y. Liu, V. Novak, On the origin of Lüders-like deformation of NiTi shape memory alloys. J. Mech. Phys. Solids **53**, 1719–1746 (2005)
9. X. Balandraud, E. Ernst, E. Soós, Rheological phenomena in shape memory alloys. C.R. Acad. Sci., Ser. IIb: Mec., Phys., Chim., Astron. **327**(1), 33–39 (1999)
10. X. Balandraud, A. Chrysochoos, S. Leclercq, R. Peyroux, Influence of the thermomechanical coupling on the propagation of a phase change front. C.R. Acad. Sci., Ser. IIb: Mec. **329**, 621–626 (2001)
11. D. Delpueyo, X. Balandraud, M. Grédiac, S. Stanciu, N. Cimpoesu, A specific device for enhanced measurement of mechanical dissipation in specimens subjected to long-term tensile tests in fatigue. Strain **54**, e1225 (2018)
12. A. Chrysochoos, H. Louche, An infrared image processing to analyse the calorific effects accompanying strain localisation. Int. J. Eng. Sci. **38**(16), 1759–1788 (2000)
13. V. Delobelle, D. Favier, H. Louche, N. Connesson, Determination of local thermophysical properties and heat of transition from thermal fields measurement during drop calorimetric experiment. Exp. Mech. **55**, 711–725 (2015)
14. P. Jongchansitto, C. Douellou, I. Preechawuttipong, X. Balandraud, Comparison between 0D and 1D approaches for mechanical dissipation measurement during fatigue tests. Strain **55**, e12307 (2019)
15. C. Zanotti, P. Giuliani, A. Chrysanthou, Martensitic-austenitic phase transformation of Ni-Ti SMAs: Thermal properties. Intermetallics **24**, 106–114 (2012)
16. D. Delpueyo, X. Balandraud, M. Grédiac, Heat source reconstruction from noisy temperature fields using an optimised derivative Gaussian filter. Infrared Phys. Technol. **60**, 312–322 (2013)
17. H. Louche, Analyse par thermographie infrarouge des effets dissipatifs de la localisation dans des aciers. Mécanique [physics.med-ph], Université Montpellier II - Sciences et Techniques du Languedoc, 1999 (in French)
18. J. Pilch, L. Heller, P. Sittner, Final thermomechanical treatment of thin NiTi filaments for textile applications by electric current, in *ESOMAT 2009 - 8th European Symposium on Martensitic Transformations Prague*, EDP Sciences, vol 05024 (2009). https://doi.org/10.1051/esomat/200905024